
Study and Develop the Thai-Made Irrigation Pump System (Tor Payanak) in a Large Aquaculture Pond

Kasantikul, B.^{1*} and Laksitanonta, S.²

¹Mechanical Engineering, Department of Mechanical Engineering, Faculty of Engineering, Kasetsart University ²Mechanical Engineering, Department of Mechanical Engineering, Faculty of Engineering, Kasetsart University, Thailand.

Kasantikul, B. and Laksitanonta, S. (2014). Study and develop the thai-made irrigation pump system (Tor Payanak) in a large aquaculture pond. International Journal of Agricultural Technology 10(5):1115-1138.

Abstract The objectives of this research were to design and simulate the flow phenomena in the Thai-made Irrigation Pump (TmIP) using Ansys CFX software to numerically analyze and study the flow phenomena and also to determine the effects of geometric factors on the TmIP efficiency. Such geometric characteristics of the impeller as the inlet and outlet angles, the number of blades, the length of the blade and the height of Hub of the impeller affected the total head pressure, flow rate and efficiency of the TmIP. For TmIP with 6-inch impeller, the optimum design of geometry parameters are: the number of blades 6 blades, the length of the blade 120 mm, the height of Hub 45 mm, inlet angle 54° and outlet angle 68°. There will be less pressure and velocity losses for this optimum design since there is minimum circulation of vortex over the operating speed of 700-1,100 rpm. Results of the experiment showed that the properly designed impeller could increase the performance of the TmIP. Thus, in the original TmIP with 6-blade impeller, the efficiency was 56.08% at a speed of 1,000 rpm, the flow rate was 57.70 l/s, total head pressure 4.28 m., whereas in the newly designed TmIP, the efficiency is 69.65% the speed of 1,100 rpm, the flow rate 50.53 l/s, total head pressure 4.82 meters, the efficiency is increased 13.57%; the flow rates is decreased 12.43% and the total head pressure is increased 12.86%.

Keywords :Thai-made irrigation pump, CFD, Impeller

Introduction

Presently, TmIP has played an important role in Thai farming and irrigation systems. This can be evidently seen from the annually increasing number of them as found and used either in paddy fields, vegetable and fruit orchards, or aquatic farms. This is also because of the TmIP's advantages of being cheap in price, easy to use and maintain, convenient to move and simple for even a small factory to produce to use. Debriddhi pump is suitable for pumping water from the water which is lower from the located shore not

* **Corresponding author:** Kasantikul, B.; **E-mail:** fengbyk@ku.ac.th

exceeding 1-4 meters. If the water level is lower than this, the amount of pumped water would be small, not worthwhile with the investment. Therefore, the TmIP is very popular for water pumping in the paddy fields and aquatic farms.

The design of TmIP to acquire high efficiency requires understanding and studying on the internal flow behavior of pump. The studying rested on numerical and computer model is an option to study such behavior. Erik *et al.* (2001) applied Fluent Code, computer program, to predict the capacity of pump by presenting various forecasting techniques e.g. Multi Reference Frame (MRF), Mixing Plane (MP), and Sliding Mesh (SM) to compare them with the experimental results. It was found that Steady Method (MRF and MP) carries less validity compared with that of Unsteady Method (SM) which can precisely predict the capacity of pump and clearly reveal its internal flow behavior. Subsequently, Weidong *et al.* (2003) simulated the flow on computer with Ansys CFX Code and K-epsilon Model to study the velocity flow field and pressure in impellers, and to compare the influence of shapes of impellers between 6 twist blade and 4 straight blades towards velocity flow field of impeller and capacity of pump. The recirculation was found at the middle of blade to blade passage. This reason makes twist blade achieve higher efficiency than that of the straight blade. Later in 2007, Cheah *et al.* (2007) used Ansys CFX Code and k-epsilon ($k-\mathcal{E}$) turbulence model to simulate the flow to study the patterns of flow and pressure flow field in the pump at the design and off-design points. At the design points, it was found that the velocity flow field of blades was relatively smooth. There were also flow separation at the leading edge and vertical flow structure both in single structure and double structure in pump passages. As for the off-design points, the violent circulation was found at the middle of blade passage which caused flow blockage, leading to the reduction in its efficiency.

The above-mentioned significance is the background of research. The previous researches showed that the flow simulation in computer could demonstrate the flow behavior clearly and it was also a great tool for the design. However, the experimental results would measure and indicate the accuracy of flow simulation in computer. That is, the experimental results would be compared to the simulation results. This research aims to study the influence of number of blades towards the capacity of TmIP with the pattern of mixed flow by simulating the flow in computer based on Commercial CFD Code called ANSYS CFX[®] with Navier-Stokes and k- \mathcal{E} Turbulence Model in order to explore the velocity flow field and pressure in the flow passage. However, the experimental results would measure and indicate the accuracy of flow simulation in computer. That is, the experimental results would be compared to

the simulation results. And then find the optimum design. This research contains 4 main parts as the following.

The influence of number of blades

The influence of length of blades

The influence of height of hub

The cavitations of blades

Related Theories

The equation for incompressible fluid

This research selected shear stress transport $k-\omega$ to simulate the flow based on the momentum equation as below.

$$\frac{\partial}{\partial t}(\rho k) + \frac{\partial}{\partial x_i}(\rho k u_i) = \frac{\partial}{\partial x_j} \left(\Gamma_k \frac{\partial k}{\partial x_j} \right) + G_k - Y_k + S_k \quad (1)$$

The conservation equation of mass and momentum

The 3-D Reynolds averaged compressible Navier–Stokes equations with standard $k-\mathcal{E}$ turbulence is a resolution in commercial package software of ANSYS CFX[®] [8] with the conservation equation of mass and momentum as below.

$$\frac{\partial}{\partial x_i}(\rho u_i) = 0 \quad (2)$$

$$\frac{\partial}{\partial x_j}(\rho u_i u_j) = -\frac{\partial P}{\partial x_i} + \frac{\partial}{\partial x_j} \left[\mu \left(\frac{\partial u_i}{\partial x_j} + \frac{\partial u_j}{\partial x_i} - \frac{2}{3} \delta_{ij} \frac{\partial u_l}{\partial x_l} \right) \right] \quad (3)$$

$$+ \frac{\partial}{\partial x_j} \left[\mu \left(\frac{\partial u_i}{\partial x_j} + \frac{\partial u_j}{\partial x_i} \right) - \frac{2}{3} \left(\rho k + \mu_t \frac{\partial u_l}{\partial x_l} \right) \delta_{ij} \right]$$

ρ is density u (kg/m^3) is speed (m/s), p is pressure (Pa), k is turbulence kinetic energy (m^2/s^2) μ is dynamic viscosity ($\text{kg/m}\cdot\text{s}$), μ_t turbulent viscosity ($\text{kg/m}\cdot\text{s}$).

The subscripts i, j and l are directions. (x, y, z) δ_{ij} is 1 when $i = j$, or when i is not equal to j , it is 0. The conservation equation of turbulence kinetic energy (k) and dissipation ratio (\mathcal{E}) (m^2/s^2) are showed as below.

$$\frac{\partial}{\partial t}(\rho k) + \frac{\partial}{\partial x_i}(\rho k u_i) = \frac{\partial}{\partial x_j} \left[\left(\mu + \frac{\mu_t}{\sigma_k} \right) \frac{\partial k}{\partial x_j} \right] + P_k - \rho \varepsilon \quad (4)$$

$$\frac{\partial}{\partial t}(\rho \varepsilon) + \frac{\partial}{\partial x_i}(\rho \varepsilon u_i) = \frac{\partial}{\partial x_j} \left[\left(\mu + \frac{\mu_t}{\sigma_\varepsilon} \right) \frac{\partial \varepsilon}{\partial x_j} \right] + C_{\varepsilon 1} \frac{\varepsilon}{k} G_k - C_{\varepsilon 2} \rho \frac{\varepsilon^2}{k} \quad (5)$$

When σ_k and σ_ε are $k-\varepsilon$, turbulence modal is fixed number amounting to 1.0 and 1.3 respectively. P_k ($\text{kg/m}\cdot\text{s}^3$) revealed the occurrence rate of turbulent kinetic energy because of mean velocity gradient.

$$P_k = \left[\mu_t \left(\frac{\partial u_i}{\partial x_j} + \frac{\partial u_j}{\partial x_i} \right) - \frac{2}{3} \left(\rho k + 3\mu_t \frac{\partial u_i}{\partial x_i} \right) \delta_{ij} \right] \frac{\partial u_j}{\partial x_i} \quad (6)$$

Cavitation Model

VOF model is used to simulate flow with cavitation when local pressure decrease below vapor pressure. It is an effective model that used in Ansys, 2009; Lifante and Frank, (2008). This model applied Rayleigh-Plesset (RP) equation with the assumption that thermal and mechanical equilibrium exists between the phases. The RP equation provides the basis for the rate equation controlling vapor generation and construction that can be solved by a volume of fluid (VOF) volume fraction with source term. The general advection-diffusion equation for the mass fraction of an individual component is given by Ansys, 2009; Lifante and Frank, (2008).

$$\frac{\partial}{\partial t}(\rho y_i) + \frac{\partial}{\partial x_j}(\rho u_j y_i) = \frac{\partial}{\partial x_j} \left(\Gamma_{i,eff} \frac{\partial y_i}{\partial x_j} \right) + S_{y,i} \quad (7)$$

The mass fraction conservation equation transformed to terms of a volume fraction equation as shown below

$$\frac{\partial}{\partial t}(\rho_i \alpha_i) + \frac{\partial}{\partial x_j}(\rho_i u_j \alpha_i) = S_{\alpha_i} \quad (8)$$

To compute the rate of vapor generation and condensation, Rayleigh-Plesset has been used to derive source term. The rate of vaporization is given by

$$\dot{m}_v = N \rho_g \frac{dV_B}{dt} \quad (9)$$

and the rate of change of bubble volume is

$$\frac{dV_B}{dt} = \frac{d}{dt} \left(\frac{4}{3} \pi R_B^3 \right) \quad (10)$$

The Rayleigh Plesset equation describing the growth of a gas bubble in liquid is given by

$$R_B \frac{d^2 R_B}{dt^2} + \frac{3}{2} \left(\frac{dR_B}{dt} \right)^2 + \frac{2\sigma}{R_B} = \frac{p_v - p}{\rho_l} \quad (11)$$

where R_B represents the bubble diameter, p_v is the pressure in the bubble, p is the pressure in the liquid surrounding the bubble and σ is the surface tension coefficient between the liquid and vapor.

Validation

In terms of validation, we tested the accuracy of the model by comparing calculated results with experimental results in simple shapes (2-D and 3-D hydrofoil) because they use less resource and save time in computing than the runner turbine, and many researches made about hydrofoil are reliable Youcef (2006). Since validation was proven, the simulation of cavitation flow on a bulb turbine was calculated in the next step. The application is a NACA0009 hydrofoil, truncated at 90% of the original chord length. It has the final dimensions of 100 mm of chord length. The 3D test section is modeled by a quasi 2D domain, with five rows of cells in spanwise direction for the numerical domain. The density of bubbles and the initial radius has been adjusted and fixed for all this study, $n_0 = 1018 \text{ B/m}^3$, $R_0 = 10^{-6} \text{ m}$. The computed domain (Fig. 2) is characterized by 9 blocks with C-type grid of (5×88000) mesh cells. The boundary conditions are set using a velocity inlet ($C_{ref} = 20 \text{ m/s}$) and a pressure at the outlet (the parameter which fixes the cavitation coefficient σ). Knowing that the cavity is located on the suction side of the hydrofoil, when cavitation occurs evidently. Figure 3-5 shows that the vapor volume fraction computed by the proposed cavitation model (with standard k- ϵ turbulence model) so we can conclude that it allow to design correctly the cavity shape. Figure 3-5 shows that the new model is on a good concordance with experimental results and it is able to evaluate correctly the evolution of the shape of cavity with decreasing σ .

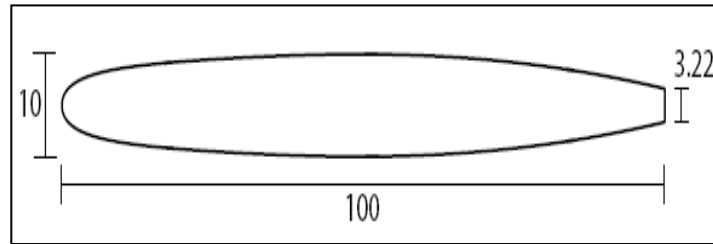


Fig. 1. NACA0009 Hydrofoil

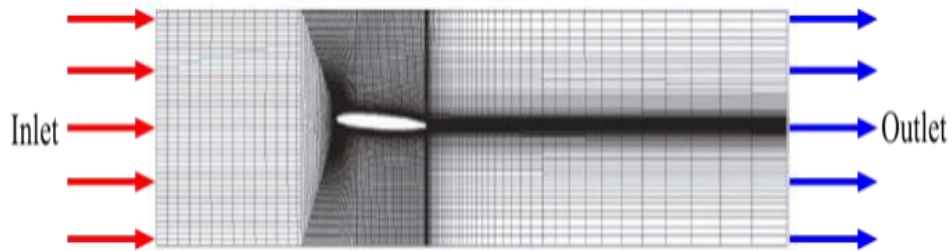


Fig. 2. NACA0009 domain grid

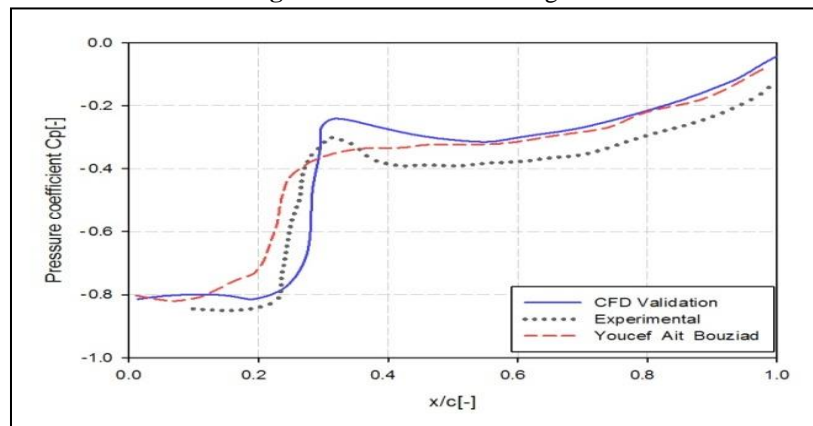


Fig. 3. Numerical result and experimental (on NACA0009, $i=2.5^\circ$, $\sigma=0.85$) Youcef (2006).

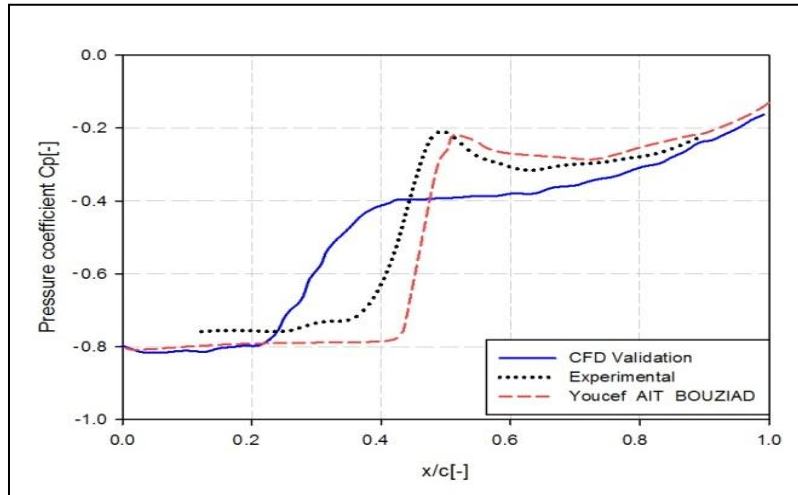


Fig. 4. Numerical result and experimental (on NACA0009, $i=2.5^\circ$, $\sigma=0.75$) Youcef (2006).

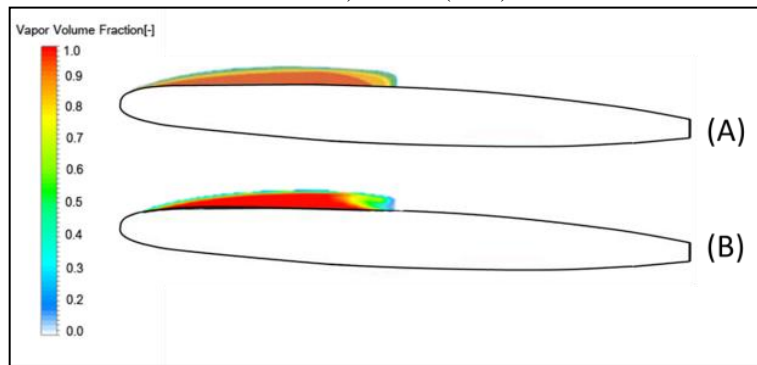


Fig. 5. Pressure distribution and cavity shape on NACA0009 $i=2.5^\circ$, $\sigma=0.75$, (A) from Youcef (2006) B(from Validation

The Features of TmIP

The TmIP is presented in figure 6. The TmIP had a round tube. The inside had the fixed long axle. The end of one axle was connected to power engine. The other side of it is connected to blade and put under the water. The TmIP pumps the water through the tube by the impeller. The impeller of TmIP take the water inward.

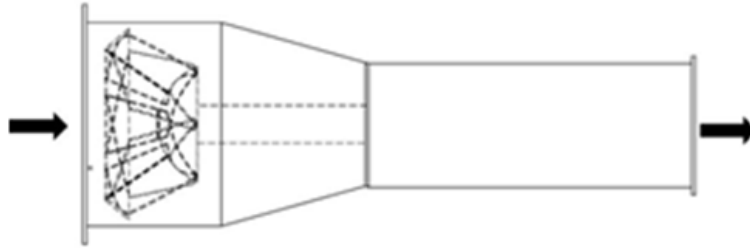


Fig. 6. Thai-made Irrigation Pump (TmIP)

Computational Fluid Dynamics)CFD(

This research adopted Ansys CFX Code (2006). It is prevalently applicable software to simulate the internal flow of turbo machine in order to study 3D Turbulence with the equation of Navier-Epsilon Turbulence Model (Weidong *et al.*, 2003; Andrej and Ignacijo, 2003; Zhang, 2006) for precise calculation, good detailed structure of velocity flow field in blade to blade passage, and flow on boundary layer. Consequently, 963,760 tetrahedral cells Ansys CFX Code (2006) were built at blades. The number of created cells in this research was compared to those in the previous researches (Miner, 2005; Goto *et al.*, 2002; Kaewprakaisaengkul, 1996). It was found that the number of cells used in calculation was adequate for the simulation of internal flow of impeller. The number of convergence criteria of RMS (Root mean square) residual of mass/momentum equation and epsilon equation was fixed at 1.0e-04 Ansys CFX Code (2006).

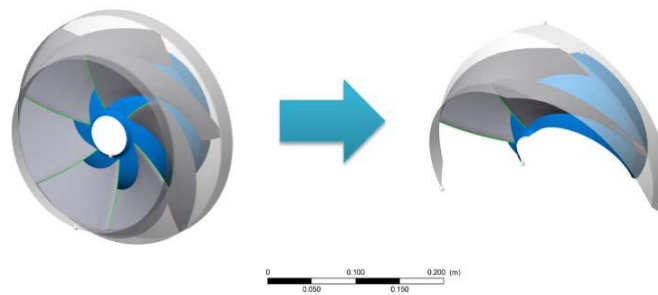


Fig. 7. Impeller

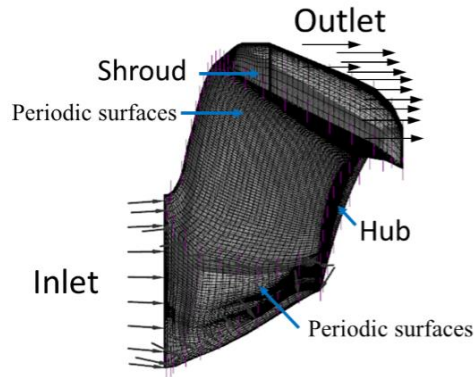


Fig. 8. Tetrahedral Cell

Table 1. Specifications of impeller of TmIP

Details	Size
Diameter of blade (mm)	234
Diameter of inlet (mm)	255
Diameter of outlet (mm)	155
Number of blades	4,5,6

Boundary Conditions

Steady flow

Incompressible flow

Density constant with water density of 998.2 kg/m³

Viscous flow with water viscosity of 0.001003 kg/m

Turbulent flow by using stress transport equation of $k - \omega$ in the flow simulation by determining intensity of turbulent flow and hydraulic radius

5% Intensity of turbulent flow

Pressure Inlet

Outlet with fixed pressure

Stationary wall and no-slip condition with 700,800,900,1000, and 1100 revolution per minute (rpm)

Results and discussions

The influence of number of blades towards efficiency

This aims to study the influence of number of blades towards the capacity of TmIP. The blades carry 234 mm in diameter with the changes to 4, 5, and 6 blades.

The impacts caused by the number of blades (4, 5, and 6 blades) towards the pressure flow field and the velocity flow field of TmIP were as the following.

Table 2 Comparison on the result of numerical simulation of 4, 5, and 6 blades

Speed (rpm)	4 Blades			5 Blades			6 Blades		
	H (m)	Q (l/s)	Eff (%)	H (m)	Q (l/s)	Eff (%)	H (m)	Q (l/s)	Eff (%)
700	1.67	38.74	20.65	1.753	28.30	22.761	1.89	28.74	30.81
800	2.64	42.53	22.33	2.755	41.37	38.461	2.87	42.53	41.95
900	3.24	52.76	27.83	3.426	49.87	46.441	3.63	49.757	50.07
1000	3.46	56.36	30.92	4.351	55.73	47.543	4.67	55.36	52.17
1100	4.07	60.23	32.04	4.753	58.24	45.325	5.26	57.23	51.26

Pressure flow field of blade to blade passage

According to the flow simulation as showed in figure 9, it can be noticed that in terms of the pressure distribution of blade to blade passage at the middle of width of B4 (4 blades) outlet on suction side, the pressure decreased in wide area which almost covered the middle of blade's length. This was highly different compared with the pressure in leading edge on pressure side of blade. When comparing this with B5 (5 blades) and B6 (6 blades), as the number of blades are higher, their blade passages are narrower. As a result, the difference of pressures between pressure side and suction side was lower. The simulation results clearly showed that the number of blades influenced the pressure distribution of passages and difference in pressures between the pressure side and suction side of impeller.

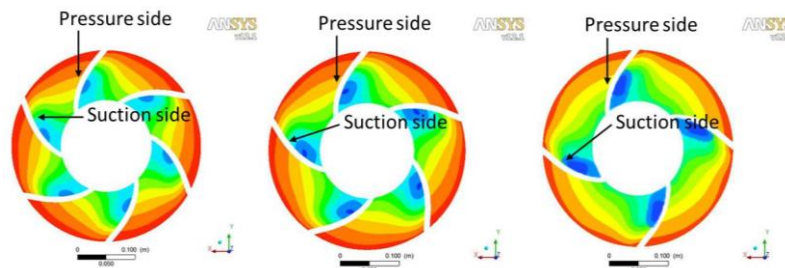


Fig. 9. The pressure distribution of 6, 5, and 4 blades at 80% span

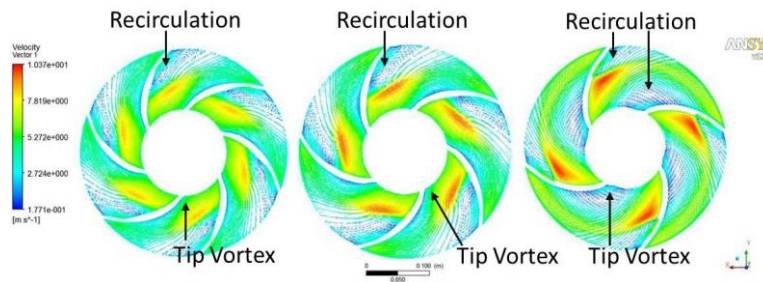


Fig. 10. The velocity flow field of 6, 5, and 4 blades at 80% span

Velocity flow field of blade to blade passage

From figure 10, the tip vortex at flow separation of leading edge on suction side can be noticed because the direction of actual flow did not follow the leading edge angle. This caused slant when the flow crashed with leading edge of 6 blades. This picture showed that the increased number of blades helped reduce the tip vortex because the eye area was narrower. Therefore, the possibility that the water would flow at the leading edge angle was lower. The flow simulation in computer at the leading edge revealed the difference the flow speed in passage. The flow speed at suction side was faster than that of the pressure side. While the flow speed of pressure side started to decrease from the leading edge to the trailing edge because the lower speed hindered the fluid not to be able to flow outside from the centrifugal force, the fluid had recirculation following blade to blade passage violently with B4 (4 blades). Then, the recirculation decreased due to the increase in blades. The increased blades made the passage narrower. The high recirculation occurred in B4 (4 blades).

The influence of geometry parameter impacting on efficiency

The research aimed to study the length of blade (L) and height of Hub (H) which affect the efficiency of TmIP.

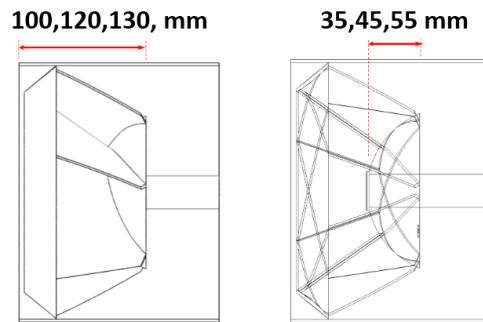


Fig. .11 Variations of the length of blade (L) and the height of Hub (H)

The increase or decrease in the length of blade (L) and the height of Hub (H)

The increase or decrease in the length of blade (L) and the height of Hub (H) may affect the flow rate, head, or even the efficiency of TmIP. This is because the increase in the length of blade (L) extended the distance of flowing fluid and the increase in the height of Hub (H) changed the size of passage area. They caused changes to the pattern of water flow. The study on influence of the length of blade (L) which affected the capacity of TmIP determined the conditions of scope of analysis. The variations were the length of blade (L) of 100, 120, and 130 mm and the height of Hub (H) of 35, 45, and 55 mm as showed in figure 11.

Table .3 The results of numerical simulation of the length of blade (L) at 100, 120, and 130 mm

Speed (rpm)	100 mm			120 mm			130 mm		
	H	Q	Eff	H	Q	Eff	H	Q	Eff
	(m)	(l/s)	(%)	(m)	(l/s)	(%)	(m)	(l/s)	(%)
700	1.96	22.10	26.64	1.89	27.20	30.76	2.05	32.10	28.69
800	2.56	38.10	32.76	2.88	40.10	42.91	2.71	41.10	30.75
900	3.24	44.20	39.85	3.64	48.20	54.03	3.47	49.80	44.78
1000	4.01	50.20	35.94	4.28	52.20	51.13	4.32	52.90	46.80
1100	4.86	53.54	35.01	5.60	56.81	51.22	5.26	57.01	48.81

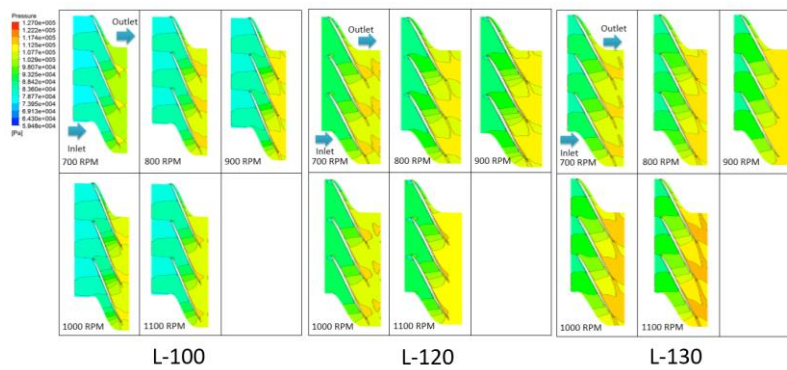


Fig. 12. The pressure flow fluid (span 50%) with the length of blade (L) at 100, 120, and 130 mm

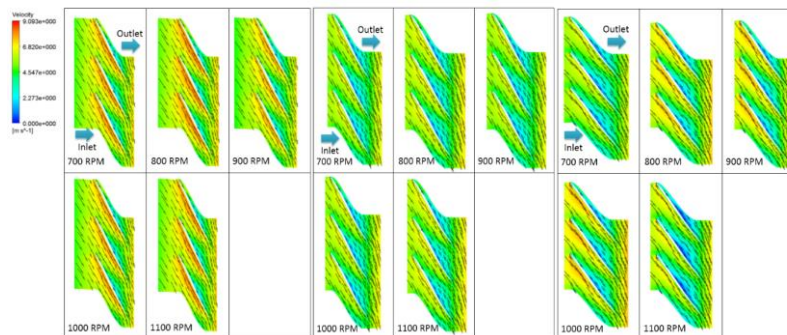


Fig. 13. The velocity flow fluid (span 50%) with the length of blade (L) at 100, 120, and 130 mm

The table 3 showed that the length of blade (L) affected head pressure, flow rate and efficiency. From figure 12, when the length of blade (L) increased, head pressure would rise as well. However, the total head pressure was maximized at 120 mm L which was similar to that of 130 mm L. When

considering the effect of the length of blade (L) per flow rate and efficiency based on table 3, it was found that 130 mm L enabled the fastest flow while 100 mm L caused the slowest flow. Nevertheless, the relations moved into the same direction. In terms of the effect of L per efficiency, the efficiency rose when the length of blades (L) were 120 mm and 130 mm. The efficiency was maximized with 120 mm L. In this regard, the study on influence of the length of blade (L) affecting pressure flow field and velocity flow field of TmIP with different length of blade (L) revealed that short blades and long blades which were not matched with the ratio of diameter per length of impeller had higher recirculation. In the passage of pressure side at the middle of blade to outlet showed violent recirculation with 130 mm L. The recirculation provoked the highest violence when TmIP work at low flow rate. The 100 mm L shortened the flow which brought about high recirculation, tip-vortex, and recirculation. These two phenomena caused loss energy which reduced the efficiency of TmIP. The 120 mm L provided higher efficiency than those of 100 mm L and 130 mm L.

Table 4. Comparison on the results of numerical simulation of the height of Hub

Speed (rpm)	35 mm			45 mm			55 mm		
	H (m)	Q (l/s)	Eff (%)	H (m)	Q (l/s)	Eff (%)	H (m)	Q (l/s)	Eff (%)
700	1.89	33.10	27.35	1.89	28.01	30.81	2.08	22.36	29.96
800	2.57	43.80	36.47	2.88	48.30	41.95	2.72	38.70	40.06
900	3.13	49.61	42.59	3.63	48.37	50.07	3.25	42.37	48.14
1000	3.87	53.05	46.68	4.28	59.50	52.17	3.96	51.02	51.21
1100	4.69	56.47	48.76	5.70	56.34	51.26	5.16	52.65	50.27

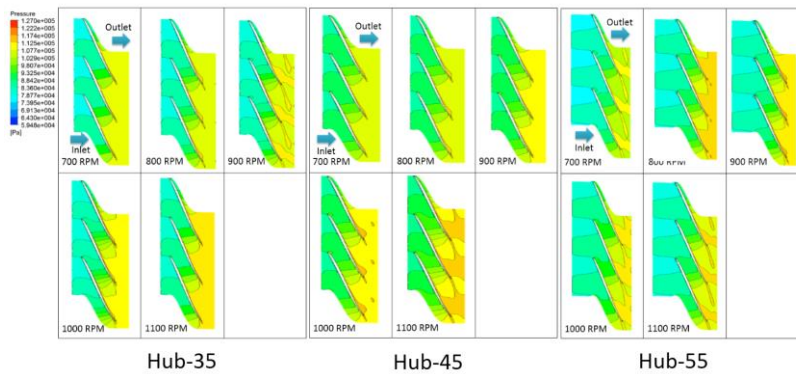


Fig. 14. Pressure flow field (span 50 %) at the height of Hub (H) of 35, 45 and 55 mm

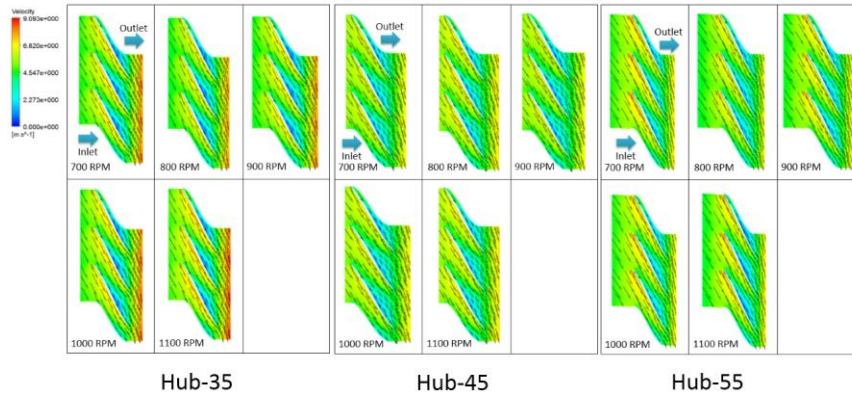


Fig. 15. Pressure flow field (span 50 %) at the height of Hub (H) of 35, 45 and 55 mm

The table 4 displayed that the height of Hub (H) affected head pressure, flow rate and efficiency as showed in figure 14. When the height of Hub (H) were 35 and 55 mm respectively, head pressure moved up. Nonetheless, 45 mm H caused the highest head pressure. In terms of the height of Hub (H) per flow rate as displayed in table 4, 45 mm H and 55 mm H had corresponding trend of relation. Nevertheless, 45 mm H enabled the highest rpm per flow rate. In this regard, the study on influence of different H affecting pressure flow field and velocity flow field inside TmIP revealed that at 35, 45, and 55 mm H when H was low, its flow rate was high. As a result, the head pressure was lower. This can be seen from the graph presenting the speed in inlet to outlet. The 45 mm H had less change from the inlet to outlet and the recirculation was less. Consequently, 45 mm H provided higher capacity compared with those of 35 and 55 mm H.

The changes of inlet blade angle and outlet blade angle

The increase or decrease of inlet blade angle and outlet blade angle may directly affect the flow pattern of impeller. If the inlet blade angle and outlet blade angle are not appropriate, they will cause recirculation in the passage which directly impacts the efficiency of pump. The study on the inlet blade angle and outlet blade angle at this time determined the conditions of scope of analysis with the inlet blade angles of 54 °, 59 ° and 64 ° and outlet blade angle of 63 °, 68 °, and 73 ° as showed in figure 16.

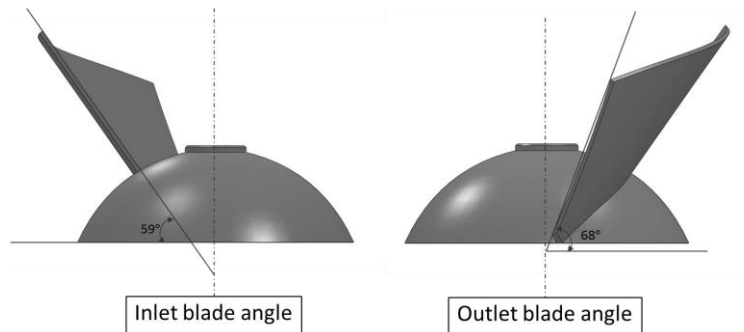


Fig. 16. Inlet blade angle and outlet blade angle

Table 4. Comparison on numerical simulation of inlet blade angle of 54 °, 59 ° and 64 °

Speed (rpm)	54 °			59 °			64 °		
	H (m)	Q (l/s)	Eff (%)	H (m)	Q (l/s)	Eff (%)	H (m)	Q (l/s)	Eff (%)
700	1.89	29.34	30.19	1.89	26.74	30.81	1.89	22.10	30.33
800	2.47	48.10	41.09	2.87	41.23	41.95	2.67	40.24	41.44
900	3.13	51.63	50.00	3.63	49.06	50.07	3.53	46.78	50.53
1000	4.07	58.16	52.04	4.67	54.67	52.17	4.87	52.97	52.11
1100	5.19	58.14	51.30	5.26	56.72	51.26	5.39	55.30	51.68

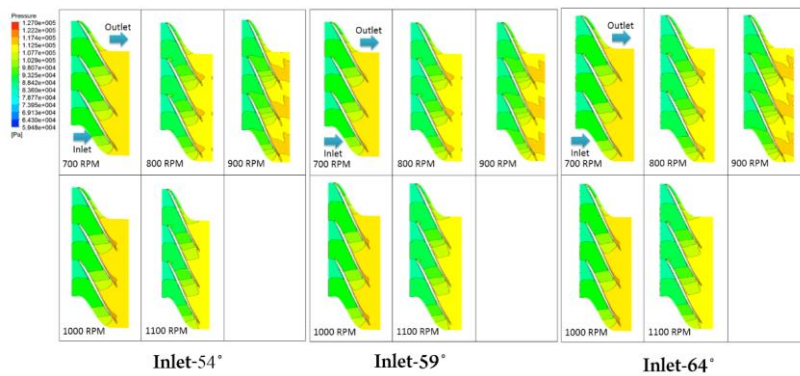


Fig. 17. Pressure flow field (span 50 %) of inlet blade angles of 54 °; 59 °and 64 °

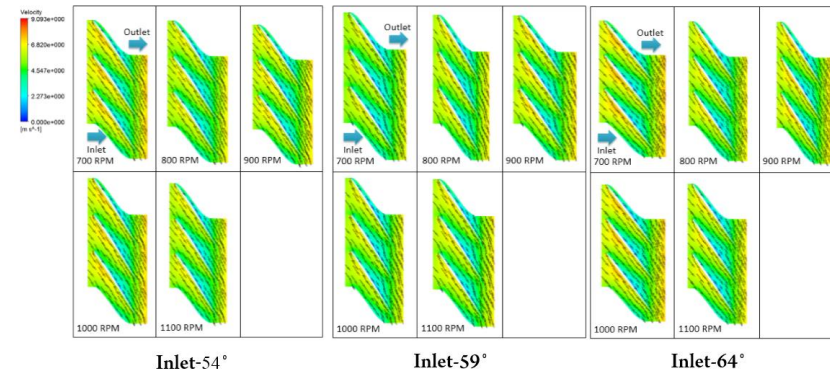


Fig. 18. Velocity flow field (span 50 %) of inlet blade angles of 54 °; 59 °; and 64 °

The table 4 showed that the inlet blade angle affected the head pressure, flow rate and efficiency. From figure 17, when the inlet blade angle increases, the head will increase too in case of inlet blade angles of 54 °, 59 ° and 64 ° respectively. However, the outlet blade angles of 59 ° and 64 ° provided similar head. When considering the result of rpm per flow rate in figure 17, it was found that the inlet blade angle of 54 ° maximized the flow rate, while the inlet blade angle of 64 ° minimized the flow rate. Nonetheless, the trends of flow rates were corresponding. As for the results of inlet blade angle per efficiency in figure 17, they revealed that when the inlet blade angles were 54 °, 59 ° and 64 °, their efficiency similarly moved towards the same direction which almost became the same line. The study on the influence of inlet blade angle affecting the pressure flow field and velocity flow field of TmIP with different inlet blade angles found that the inlet blade angles of 54 °, 59 ° and 64 ° had similar recirculation in the passage on pressure side at the middle of blades to the outlet. Consequently, the efficiency of TmIP with three inlet angles was extremely similar. However, the study on the influence of different inlet blade angles towards the pressure flow field and velocity flow field inside the TmIP

disclosed that head pressure increased as rpm in linear relation with the inlet blade angles of 54 ° and 59 °. At the low flow rate, the inlet blade angle of 64 ° had a change in inlet blade angles are related with rpm as linear relation. Nonetheless, head pressure was unpredictably changed when rpm rose.

Table 5. Comparison on the numerical simulation of outlet blade angles of 63 °, 68 °, and 73 °

Speed (rpm)	63 °			68 °			73 °		
	H (m)	Q (l/s)	Eff (%)	H (m)	Q (l/s)	Eff (%)	H (m)	Q (l/s)	Eff (%)
700	1.89	30.24	30.80	1.85	27.56	30.81	1.90	25.40	30.46
800	2.56	46.63	41.93	2.88	41.33	41.95	2.78	39.84	41.55
900	3.43	47.96	50.03	3.63	44.64	50.07	3.55	43.21	50.63
1000	3.99	55.80	52.13	4.27	53.88	52.17	4.09	50.64	52.09
1100	5.58	57.81	51.22	5.65	56.44	51.26	5.20	56.20	51.76

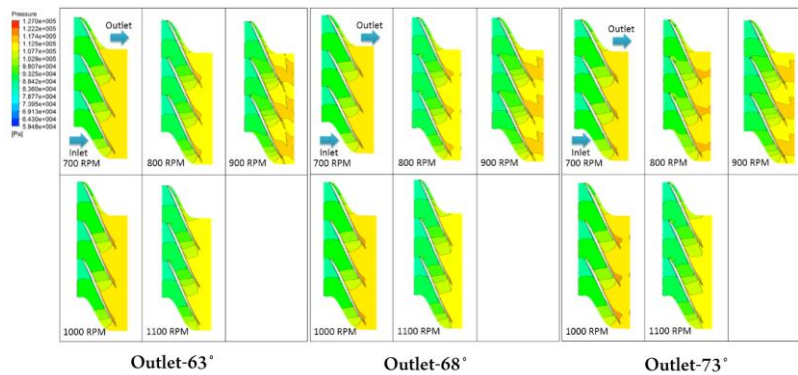


Fig. 19. Pressure flow field (span 50 %) of outlet blade angles of 63 °, 68 °, and 73 °

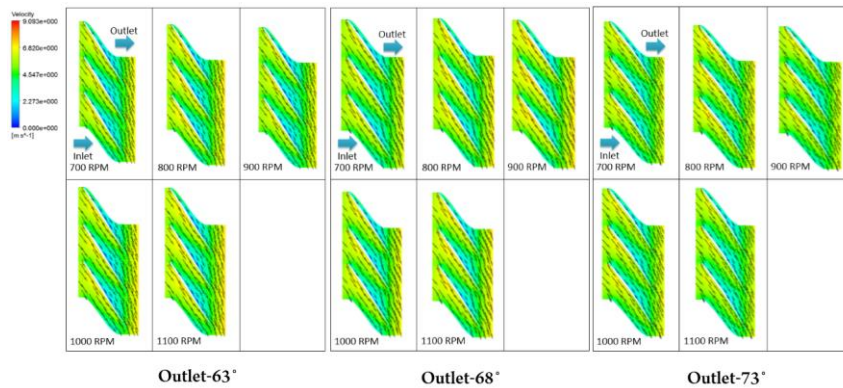


Fig. 20. Velocity flow field (span 50 %) of outlet blade angles of 63 ° ; 68 ° ; and 73 °

The Table 5 showed that the outlet blade angles impacted the head pressure, flow rate and efficiency as displayed in figure 19. When the outlet blade angle increases, the head pressure will increase with the outlet blade angles of 63 ° and 73 ° respectively. However, the outlet blade angle of 68 ° maximized the head pressure. When considering the result of rpm per flow rate as showed in figure 19, their efficiency were extremely similar and had the same trend with the outlet blade angles of 63 ° ; 68 ° ; and 73 °. In this regard, the study on influence of different outlet blade angle towards the pressure flow field and velocity flow field inside the TmIP showed the similar recirculation in the passage on pressure side at the middle of blade to the outlet with the outlet blade angles of 63 ° ; 68 ° ; and 73 °. As a result, the efficiency of TmIP with the three outlet blade angles was similar. In this regard, the outlet blade angle with 73 ° provided higher efficiency compared with those of other two angles based on the theory. Nonetheless, the study on the influence of different outlet blade angles towards the pressure flow field and the velocity flow field of TmIP showed that the head pressure increases as rpm in linear relation with the 73 ° outlet blade angle. At low flow rate, the head pressures of 63 ° and 68 ° outlet blade angles are related with rpm as linear relation. However, head pressure was unpredictably changed when rpm rose.

The study on the occurrence of cavitation in the impeller of TmIP

The NPSH value is determined by the pressure difference between the inlet pressure and the minimum pressure in the flow passage and velocity head. (Weidong, 2003; Kaewprakaisaengkul, 1996; Brennen, 1994).

$$NPSH = \frac{P_1 - P_{\min}}{\rho g} + \frac{C_1^2}{2g} \quad (12)$$

Where $C_1 = \sqrt{V_{circ}^2 + V_{neid}^2}$

Head Drop Curve

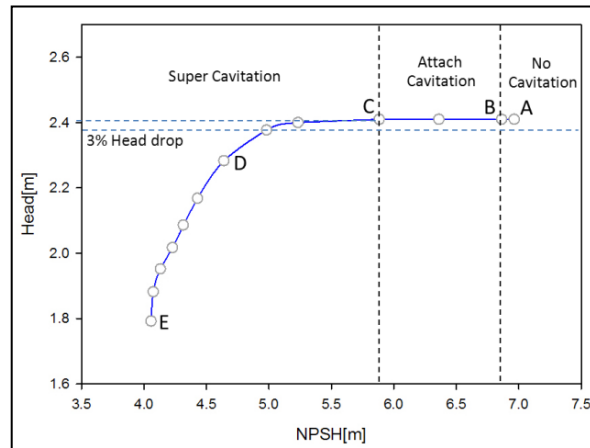


Fig. 21. Head-NPSH curve at flow rate 40 kg/s and speed 900 rpm

Figure 21: shows head drop curve as well as NPSH curve that computed by ANSYS CFX at design flow and rate speed. Volume of fluid model is selected as a cavitation model to compute rate of vapor bubble production. At inlet boundary total pressure is decreased to meet a status that cavitation formation starting. NPSH 3% is the value at which the head below 3% of no cavitation head. From head drop curve, predicted NPSH 3% can be evaluated about 4.72 m.

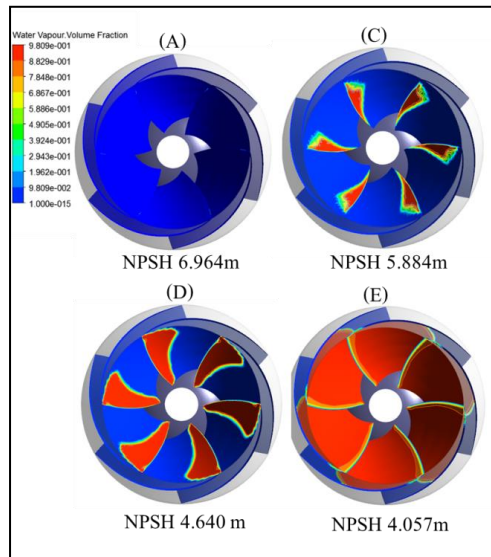


Fig. 22. VAPOR Fringe Top view speed 900 rpm and flow rate 40 kg/s

Figure 22: shows cavity length with vapor fringe plot blade to blade view which corresponds to point A, C,D and E respectively in head drop curve (Figure 1). There is no cavitation when $NPSH = 6.964$ m, attach cavitation when $NPSH = 5.884$ m and super cavitation when $NPSH = 4.640$ m, $NPSH = 4.057$ as shown in figure 9. Therefore head drop curve in figure 8 can be divided according to cavity length on blade surface into three portions as no cavitation, attach cavitation and super cavitation (Zhang, 2006). No cavitation is range from A to B in figure 8. In this portion rate of vapor production approximate zero. Attach cavitation is range B to C that has cavity length on blade surface less than or equal chord length. Cavitation on suction surface is growing when decreasing NPSH. If cavity length grow up more than chord length, super cavitations occur as shown in figure 8-D. Super cavitation is range C to E in figure 8.

Location of Cavitation

To describe a change in the location of cavitation while NPSH value is decreased, the predicted bubble vaporization rate in the flow passage is shown.

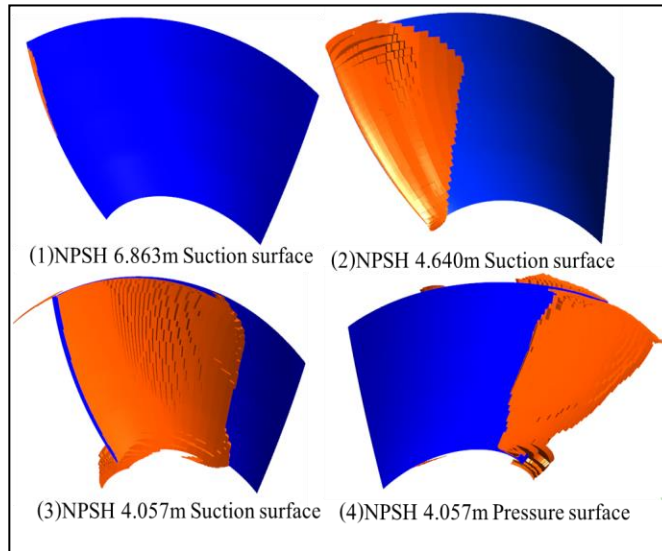


Fig. 23. Fringe Plot showing cavitation on blade surface at speed 2400 rpm, flow rate 18 kg/s

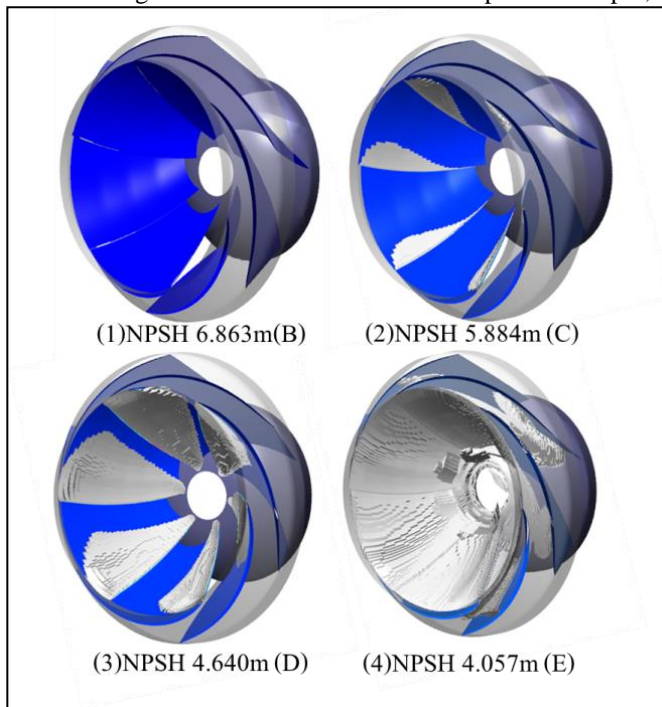


Fig. 24. Shows quantity of cavitation that occurs on impeller at 900 rpm, 40 kg/s of mass flow rate.

- (1) Inlet Total Pressure 7.0×10^4 Pa
- (2) Inlet Total Pressure 5.0×10^4 Pa
- (3) Inlet Total Pressure 3.4×10^4 Pa
- (4) Inlet Total Pressure 2.0×10^4 Pa

Figure 23: shows VAPOR Fringe Plot with variation of NPSH. Figure 23-1 shows that the maximum evaporation rate occurred at the blade leading edge near the tip. Figure 23-2 shows that the location of maximum evaporation rate moves from the blade leading edge. Figure 23-3 shows that the maximum evaporation rates occur at the blade trailing edge near the tip. Figure 23-4 shows that cavitation occur on the pressure surface in case of super cavitation. Hence for NPSH value lower than NPSH value that inception cavitation form, the location of maximum evaporation rate move from the blade leading edge to the blade trailing edge along the stream line near the tip. Cavitation can be seen on pressure surface as shown in figure 23-4. If cavitations occur on pressure surface, pump head corresponding point E on head drop curve figure 8 will decrease rapidly.

Figure 24: shows the calculated of cavitation quantity at 900 rpm, 40 mass flow rate and inlet total pressure 7.0×10^4 , 5.0×10^4 , 3.4×10^4 and 2.0×10^4 Pa. Inception cavitation that formation start can be approximate when inlet total pressure value was about 7.0×10^4 NPSH 6.863 m, vapor was combine and became the cavitation that called “attach cavitation” as shown in figure 24-2. Head value was stable and when inlet total pressure was 3.4×10^4 Pa and NPSH was 4.640 m, generated the super cavitating that shown in figure 11-3. The cavity length was longer than impeller, head slightly decreased and immensely decreased when NPSH was 4.057 m as shown by (E) on NPSH head curve. The decrease of head cause of the vapour was compressible, changing of head at inception cavitation that made stream line deviation. These causes affect the velocity, pressure and head was change.

Conclusion

The results of flow simulations in computer revealed that the high number of blades increased the pressure at the outlet. Moreover, the velocity flow field carried more of equal speed distribution. As for the influence of the length of blade (L), short blades and long blades which were not matched with the ratio of diameter per length of impeller had higher recirculation. In terms of the height of Hub (H), the velocity flow field and the pressure flow field in the inlet to outlet with 45 mm H carried small changes from the inlet to outlet. This caused less recirculation.

Effects of the cavitations, this study found that the cavitations occur in low pressure area, which causes high speed. The cavitations area starts from leading edge along to the tip. When NPSH is reduced, the cavitations area moves from leading edge to the trailing edge.

For TmIP with 6-inch impeller, the optimum design of geometry parameters are: the number of blades 6 blades, the length of the blade 120 mm,

the height of Hub 45 mm, inlet angle 54° and outlet angle 68° . There will be less pressure and velocity losses for this optimum design since there is minimum circulation of vortex over the operating speed of 700-1,100 rpm. Results of the experiment showed that the properly designed impeller could increase the performance of the TmIP. Thus, in the original TmIP with 6-blade impeller, the efficiency was 56.08% at a speed of 1,000 rpm, the flow rate was 57.70 l/s, total head pressure 4.28 m., whereas in the newly designed TmIP, the efficiency is 69.65% the speed of 1,100 rpm, the flow rate 50.53 l/s, total head pressure 4.82 meters, the efficiency is increased 13.57%; the flow rates is decreased 12.43% and the total head pressure is increased 12.86%.

References

- Andrej, P. and Ignacijo, B. (2003). Influence of additional inlet flow on the peroration and performance of centrifugal impellers, international association of hydraulic engineering and research 41:207216.
- Ansys CFX 12.1 (2009). ANSYS, Inc.
- Ansys CFX-Solver Theory Guide. ANSYS CFX Release 11.0, ANSYS Europe Ltd., 1996-2006.
- Brennen, C. E. (1994). Hydrodynamics of Pumps. London: Oxford University Press.
- Cheah, K. W., Lee, T. S., Winoto, S. H. and Zhao, Z. M. (2007). Numerical flow simulation in a centrifugal pump at design and off-design conditions, International of Rotating Machinery. 8 pp.
- Erik, D., Janvierendeels, S. S. and vande voorde, J. (2001). Performance prediction of centrifugal pumps with CFDTools, Scientific Bulletin of the Academic Computer Center in Gdansk 5:79-94.
- Goto, A., Nohmi, M. and Sakurai, T. (2002). Hydrodynamic design system for pumps based on 3-D CAD, CFD, and Inverse Design Method, Journal of Fluids Engineering 124:329.
- Kaewprakaisaengkul, C. (1996). Evaluation and improvement of thai-made irrigation pumps. (Ph.D. thesis). Asian Institute of Technology.
- Lifante, C. and Frank, T. (2008). Investigation of higher order pressure fluctuations and its influence on ship stern, taking into account cavitation at propeller blades, Final Report ANSYS / TR-08-04, Research Project No: 03SX202A.
- Miner, S. M. (2005). CFD analysis of the first- stage rotor and stator in a two-stage mixed flow pump. International Journal of Rotating Machinery 1:23–29.

- Weidong, Z., Zhimei, Z., Lee, T. S. and Winoto, S. H. (2003). Investigation of flow through centrifugal pump impellers using computation fluid dynamics. *International Of Rotating Machinery* 9:496.
- Youcef, A. B. (2006). Physical modelling of leading edge cavitation : computational methodologies and application to hydraulic machinery. (Ph.D. thesis). University of Paris.
- Zhang, P. (2006). Numerical simulation of influence on the mixed flow circulating pump performance curve for the structure parameters adjustment. *Journal of Energy Conservation* 286:25-27.

(Received 19 July 2014; accepted 31 August 2014)